Global variations of HDO and HDO/H_2O ratios in the upper troposphere and lower stratosphere derived from ACE-FTS satellite measurements

William J. Randel,[1] Elisabeth Moyer,[2] Mijeong Park,[1] Eric Jensen,[3] Peter Bernath,[4] Kaley Walker,[5] and Chris Boone[6]

Received 8 August 2011; revised 2 February 2012; accepted 6 February 2012; published 22 March 2012.

[1] High-quality satellite observations of water and deuterated water in the upper troposphere and lower stratosphere (UTLS) from the Atmospheric Chemistry Experiment Fourier transform spectrometer (ACE-FTS) are used to map global climatological behavior. Spatial and temporal variability in these data suggest that convection plays a significant role in setting water vapor isotopic composition in these regions. In many instances, enhancements in HDO/H_2O (i.e., δD) are closely tied to patterns of climatological deep convection and uncorrelated with water vapor, although convection appears to have different isotopic effects in different locations. The ACE-FTS data reveal seasonal variations in the tropics and allow mapping of climatological regional structure. These data reveal strong regional isotopic enhancement associated with the North American summer monsoon but not the Asian monsoon or the western Pacific warm pool. We suggest that the isotopic effects of deep convection near the tropopause are moderated by the ambient relative humidity, which controls the amount of convective ice that evaporates. Local convective signals can in turn affect global behavior: the North America monsoon influence introduces a Northern Hemisphere–Southern Hemisphere asymmetry in water isotopic composition in the lower stratosphere that extends into the tropics and influences the apparent seasonal cycle in averaged tropical UTLS data. Seasonal variation in tropical lower stratospheric water isotopic composition extends up to ~20 km in ACE retrievals, but in contrast to previous reports, there is no clear evidence of propagation beyond the lowermost stratosphere. The reliability of these observations is supported by the broad consistency of ACE-FTS averaged tropical profiles with previous remote and in situ δD measurements.

Citation: Randel, W. J., E. Moyer, M. Park, E. Jensen, P. Bernath, K. Walker, and C. Boone (2012), Global variations of HDO and HDO/H_2O ratios in the upper troposphere and lower stratosphere derived from ACE-FTS satellite measurements, *J. Geophys. Res.*, *117*, D06303, doi:10.1029/2011JD016632.

1. Introduction

[2] The isotopic composition of water vapor provides unique information about convective processes and transport in the atmosphere, and isotopes are potentially powerful diagnostics for understanding processes near the tropical tropopause, where both in situ dehydration and convective transport of water play significant roles. As water vapor condenses to liquid or ice, the heavier isotopologues (HDO, $H_2^{18}O$, $H_2^{17}O$) are preferentially removed from the vapor phase. Evaporating ice, on the other hand, can carry the more enhanced isotopic signature of lower altitudes. The isotopic signature of water vapor then provides a measure of the history of condensation and evaporation (often convolved with mixing or other effects). In the idealized situation where all condensate is removed as an air parcel slowly rises and cools (so-called Rayleigh fractionation), the deuterated isotopologue (HDO, which is strongly fractionated compared to H_2O) is depleted relative to H_2O from near-surface values by 90% near the cold tropical tropopause. However, observations suggest much less HDO depletion in the stratosphere, with isotopic depletion of about 65% [e.g., *Moyer et al.*, 1996; *Johnson et al.*, 2001], illustrating the importance of non-Rayleigh processes such as evaporation of lofted ice, mixing, and supersaturation effects. It is the

[1]National Center for Atmospheric Research, Boulder, Colorado, USA.
[2]Department of the Geophysical Sciences, University of Chicago, Chicago, Illinois, USA.
[3]NASA Ames Research Center, California, USA.
[4]Department of Chemistry and Biochemistry, Old Dominion University, Norfolk, Virginia, USA.
[5]Department of Physics, University of Toronto, Toronto, Ontario, Canada.
[6]Department of Chemistry, University of Waterloo, Waterloo, Ontario, Canada.

Copyright 2012 by the American Geophysical Union.
0148-0227/12/2011JD016632

improved understanding of such processes that fuels measurements and model simulations of the detailed behavior of HDO and other water isotopologues.

[3] Relating observed water isotopic composition to global-scale processes has been difficult because of the limitation of measurements, with aircraft measurements at high resolution but extremely limited spatial coverage, and remote measurements at greater coverage but poor vertical resolution. The mixing ratio of HDO is approximately 3000–10,000 times smaller than H_2O, and highly accurate measurements are required to quantify the detailed vertical structure from the troposphere to the stratosphere. Past observations include limited measurements from balloons or aircraft using a Fourier transform spectrometer (FTS) [e.g., *Johnson et al.*, 2001; *Coffey et al.*, 2006; *Notholt et al.*, 2010] and in situ aircraft observations [e.g., *Hanisco et al.*, 2007; *Sayres et al.*, 2010]. Some of the first tropical profile observations extending to the stratosphere were obtained from space-based FTS measurements [*Moyer et al.*, 1996; *Kuang et al.*, 2003]. More recently, satellite data have begun to map the global behavior of HDO, including observations from the Michelson Interferometer for Passive Atmospheric Sounding (MIPAS) instrument [*Payne et al.*, 2007; *Steinwagner et al.*, 2007, 2010]. *Nassar et al.* [2007] used high-quality measurements from the Atmospheric Chemistry Experiment Fourier transform spectrometer (ACE-FTS) to highlight the tropical behavior of HDO. The ACE-FTS solar occultation instrument provides limited spatial sampling, and *Nassar et al.* [2007] focused on tropical measurements for the first several years of data. ACE-FTS has continued to provide high-quality data (over 24,000 occultations to present), and in this work we use these data to document the global climatological behavior of HDO in the upper troposphere and stratosphere, including the tropical seasonal cycle (and its interannual variability) and local horizontal structure.

2. Data and Analysis

[4] The ACE mission was launched 12 August 2003 into a high inclination (74°) circular orbit at 650 km altitude [*Bernath et al.*, 2005]. The ACE-FTS instrument obtains Fourier transform absorption spectra from solar occultation measurements, with a wave number range of 750 to 4400 cm^{-1} and a resolution of 0.02 cm^{-1}. The vertical field of view of the instrument is about 3 km, with observations spanning altitudes from above 30 km (the top level of interest here) down into the troposphere (until obstructed by opaque clouds). Measurements during each occultation are obtained with a vertical sampling of 2–6 km (depending on the angle of the Earth-Sun vector with respect to the spacecraft velocity), and constituent profiles are available on an (oversampled) 1 km vertical grid [*Boone et al.*, 2005]. The data used here are based on version 2.2 retrievals and include both water vapor (H_2O) and deuterated water (HDO) profiles (the latter is based on updated version 2.2 retrievals). The HDO/H_2O ratios are characterized by their relation to that in a standard (Vienna standard mean ocean water, SMOW):

$$\delta\mathrm{D}(‰) = \left\{\left[(\mathrm{HDO}/\mathrm{H_2O})/(\mathrm{HDO}/\mathrm{H_2O})_{\mathrm{SMOW}}\right] - 1\right\} \times 1000,$$

where $(\mathrm{HDO}/\mathrm{H_2O})_{\mathrm{SMOW}} = 2 \times 1.56 \times 10^{-4}$, and δD is expressed in per mil (‰).

[5] Uncertainty in averaged isotopic profiles will be dominated by climatological variability and possibly systematics rather than random errors. For individual occultations, random error in retrieved concentrations can be 4%–6% for H_2O and 4%–11% for HDO, with a significant contribution from temperature and pressure errors common to both species, so that random errors in retrieved HDO/H_2O ratios is 3%–11%; this corresponds to 12‰–44‰ in δD for an upper tropospheric value of $\delta\mathrm{D} = -600‰$. In seasonally averaged profiles (with ~80 measurements during each season over 15°N–15°S), random error is reduced by an order of magnitude to less than 5‰. An upper bound on systematic uncertainties can be estimated by comparisons of ACE-FTS water vapor measurements to independent measurements from other sources, yielding upper bound estimates of ±18% in the upper troposphere and lower stratosphere (UTLS) region [*Carleer et al.*, 2008; *Hegglin et al.*, 2008; *Lossow et al.*, 2011]. If uncertainties are independent and equally sized across isotopologues, systematic uncertainty in UTLS δD could be as large as ±100‰. Much of any systematic error would likely manifest as a near-constant offset over a vertical extent of many kilometers. One apparent stationary feature in averaged profiles, a seasonally constant isotopic enhancement of tens of per mil near ~25 km is a known retrieval artifact in v2.2. For vertically propagating signals such as the seasonal cycle, however, it is highly unlikely that systematics could coincidently enhance or mask a signal of tens of per mil in magnitude.

[6] The V2.2 retrievals for ACE-FTS measurements cover the years 2004–2009, with over 24,000 occultations. The sampling as a function of latitude and month is shown in Figure 1; note that the measurement patterns nearly repeat each year (although the corresponding longitudinal sampling varies from year to year). The majority of the observations occur at high latitudes, but measurements cross the tropics four times per year (approximately February, April, August, and October). The overall sampling provides near-global coverage for 3 month samples, and our analyses are based on data binned for December–February (DJF), March–May (MAM), June–August (JJA), and September–November (SON). We examine all profiles for each season within various latitude bands, and omit a small number of retrieval outliers that are outside of three local standard deviations of the group. Climatological fields are constructed by combining all observations from 2004 to 2009, and we also examine year-to-year variability for some quantities. We investigate the latitude-longitude structure of seasonal (3 month) averages from the ACE-FTS data by binning the observations onto a 10° × 20° latitude-longitude grid, including a Gaussian-weighted sum of measurements within 1000 km of each grid box (using a Gaussian length scale of 750 km).

3. Results

3.1. Global Structure and Seasonality

[7] As background for examining structure in δD, the seasonal mean structure for both H_2O and HDO derived from ACE-FTS measurements during MAM are shown in Figure 2. The zonal average tropopause altitude is also indicated in Figure 2, defined as the thermal (lapse rate) tropopause over the extratropics, and the cold point tropopause

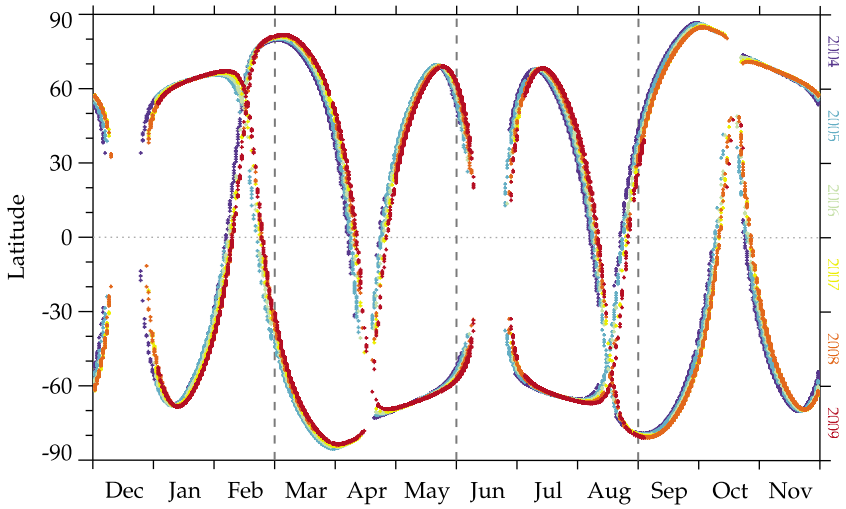

Figure 1. Latitude-month diagram illustrating the sampling of the Atmospheric Chemistry Experiment Fourier transform spectrometer (ACE-FTS) observations. Different colors represent different years; the latitudinal sampling repeats, although different longitudes are sampled each year.

over latitudes 25°N–25°S. H_2O shows the well-known climatological structure of a minimum in the tropical lower stratosphere, with relatively dry air extending latitudinally in the lower stratosphere to cover much of the globe (approximately following the 400–450 K isentropic layer). Minimum values also extend vertically into the middle stratosphere in the tropics, linked with the upward Brewer-Dobson circulation; note the secondary MAM minimum near 25 km in Figure 2a, which is the tropical minimum that originated near the tropopause from the previous year. H_2O increases with altitude and latitude in the stratosphere as a result of methane oxidation, so the spatial structure approximately mimics the stratospheric age of air [e.g., *Waugh and Hall*, 2002]. The spatial structure and magnitude of H_2O in Figure 2a is in excellent detailed agreement with other satellite observations [*Randel et al.*, 2001; *Urban et al.*, 2007; *Fueglistaler et al.*, 2009].

[8] The climatological structure of HDO (Figure 2b) is very similar to H_2O (Figure 2a) as expected, although the stratospheric mixing ratio is approximately 10,000 times

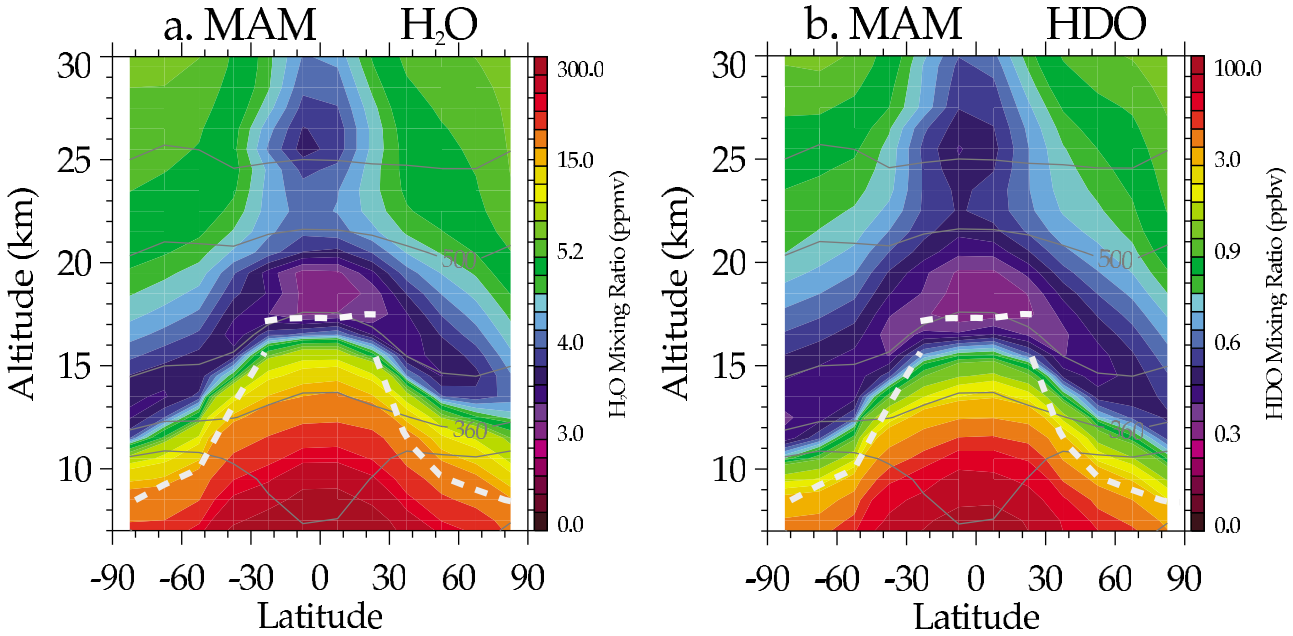

Figure 2. Meridional cross sections of (a) H_2O mixing ratio and (b) HDO mixing ratio derived from ACE-FTS observations during March–May. The dashed white line denotes the zonal average tropopause, defined using the thermal (lapse rate) tropopause over extratropics, and the cold point over latitudes 25°N–25°S. Thin solid lines are isentropes. H_2O and HDO structures are quite similar, as expected.

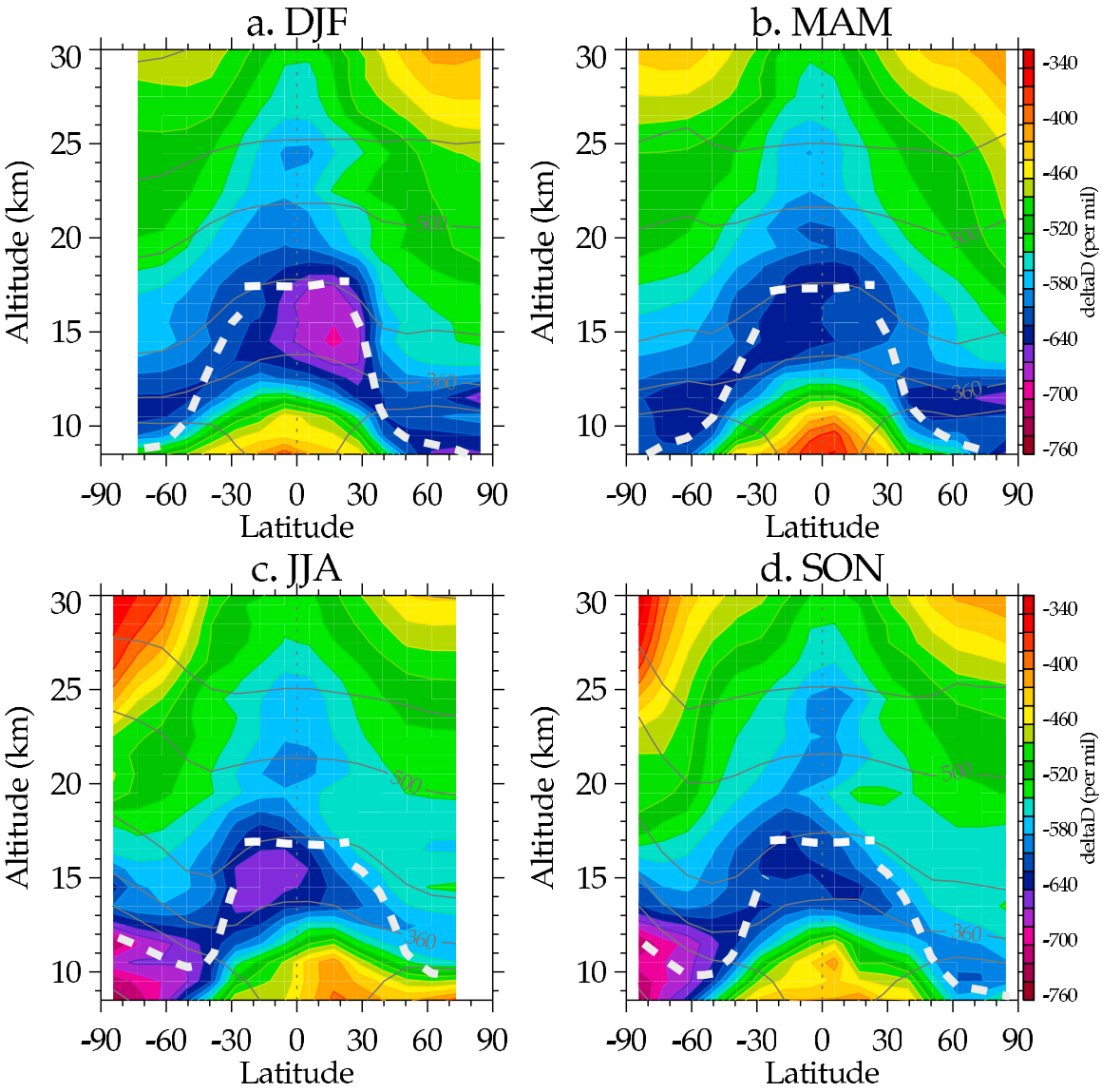

Figure 3. Meridional cross sections of δD for each of the four seasons, derived from ACE-FTS data. White dashed line denotes the tropopause, and thin solid lines are isentropes.

smaller (~0.5 ppbv for HDO versus ~4 ppmv for H_2O). As with H_2O, there is a general increase in HDO above the lower stratosphere, resulting from oxidation of CH_3D (discussed further below). The increase in HDO is slightly larger than that in H_2O, in part because methane has a heavier isotopic composition than does entering stratospheric water vapor. That difference translates to an increase in the isotopic composition δD with height and latitude in the stratosphere (Figure 3), approximately following the behavior for age of air.

[9] The isotopic composition δD also shows more subtle features not apparent in comparison by eye of HDO and H_2O distribution (Figure 3). In the troposphere δD shows the well-known decrease with height, reaching minimum values (δD ~ −650‰) near 15 km in the tropics; notably the minimum tropical values are centered significantly below the cold point tropopause (~17 km). This observed behavior is consistent with the aircraft measurements of *Hanisco et al.* [2007] and *Sayres et al.* [2010] and MIPAS observations given by *Payne et al.* [2007], as well as with previous ACE-FTS results reported by *Nasser et al.* [2007]. The larger global ACE-FTS database now allows mapping of the latitudinal structure and seasonal movements of that minimum. The upper tropospheric δD minima migrate seasonally, occurring in the winter subtropics during the solstice seasons (0–30° N during DJF and 0–30° S during JJA), and more nearly over the equator during the equinox seasons (MAM and SON). Relatively less depleted values of δD in the tropical middle troposphere (red and yellow regions in Figure 3) also move seasonally, and are aligned with the latitude of maximum convection and maximum water vapor, but the latitudinal shifts in the upper tropospheric minima are not strongly correlated with water vapor minima.

[10] The ACE-FTS data in Figure 3 do show an additional region of extremely depleted δD in the upper troposphere (~9 km) over Antarctica during JJA and SON (from

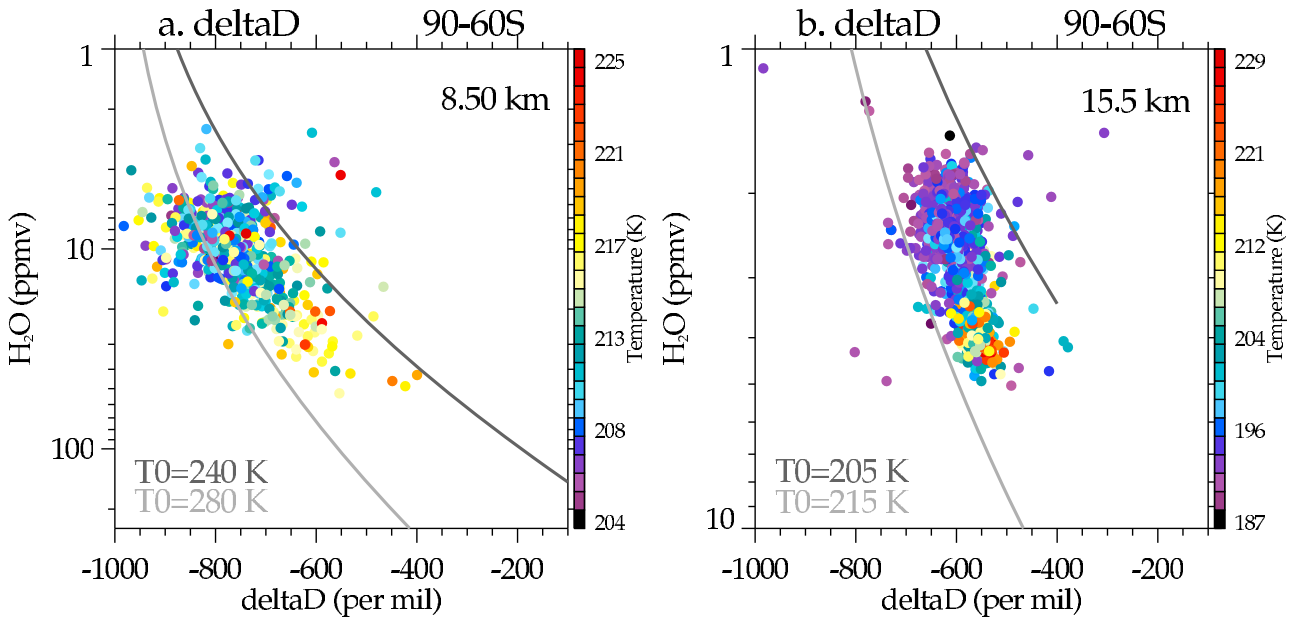

Figure 4. Scatter diagram of August–September ACE-FTS measurements of H_2O versus δD for measurements over high southern latitudes (60–90°S) at (a) 8.5 km and (b) 15.5 km. The measurements are color coded according to the coincident temperature from National Centers for Environmental Prediction reanalysis data. The superposed lines show Rayleigh curves, calculated for initial conditions of (a) T = 240–280 K, δD = 0 and (b) T = 205–215 K, δD = −400, the latter being characteristic of air in the Antarctic stratosphere during winter.

measurements during August–September, Figure 1) where δD values <−750‰ are among the lightest values measured in the Earth's atmosphere. These very low polar values of δD (∼−700‰ to −900‰) are associated with extremely dry air (H_2O ∼ 5–20 ppmv) characteristic of the Antarctic upper troposphere during winter and spring [e.g., *Vömel et al.*, 1995] (see Figure 4, which shows δD and H_2O from 60° to 90°S at 8.5 and 15.5 km). The strong depletion at 8.5 km (Figure 4a) is consistent with Rayleigh fractionation as tropospheric air moves poleward and cools, although the origin and Lagrangian history of the parcels is unknown. In contrast, air at 15.5 km, which includes the dehydrated Antarctic polar vortex, is dryer (H_2O < 2 ppmv) but less isotopically depleted (δD values not less than −700‰), consistent with this air originating in the polar stratosphere earlier in the year. The distinct δD regimes of Figures 4a and 4b demonstrate that the extremely low δD values at 8.5 km do not originate in the stratosphere, but rather are produced by in situ condensation the intensely cold Antarctic upper troposphere.

3.2. Tropical Seasonal Cycle

[11] Seasonal variations in δD are especially interesting in the tropical UTLS region, because they have been proposed as an indicator of regulation of stratospheric water vapor by dehydration at the cold point tropopause, while disruptions

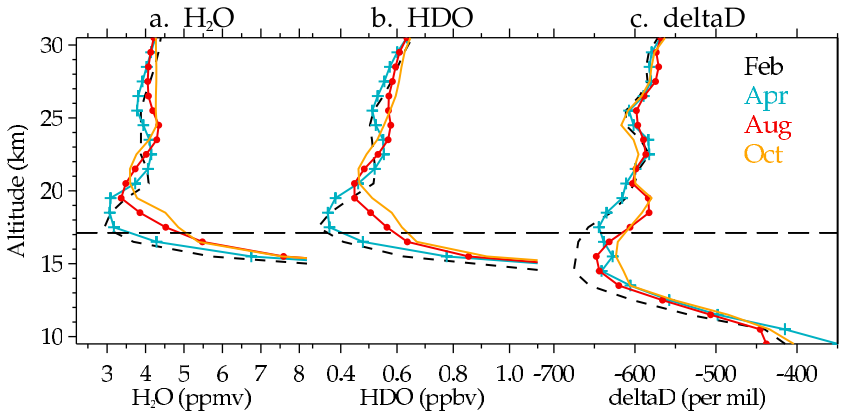

Figure 5. Climatological vertical profiles of (a) H_2O, (b) HDO, and (c) δD, derived from ACE-FTS measurements in the tropics (15°N–15°S) during February, April, August, and October (see Figure 1). The long-dashed line denotes the approximate altitude of the tropical cold point tropopause.

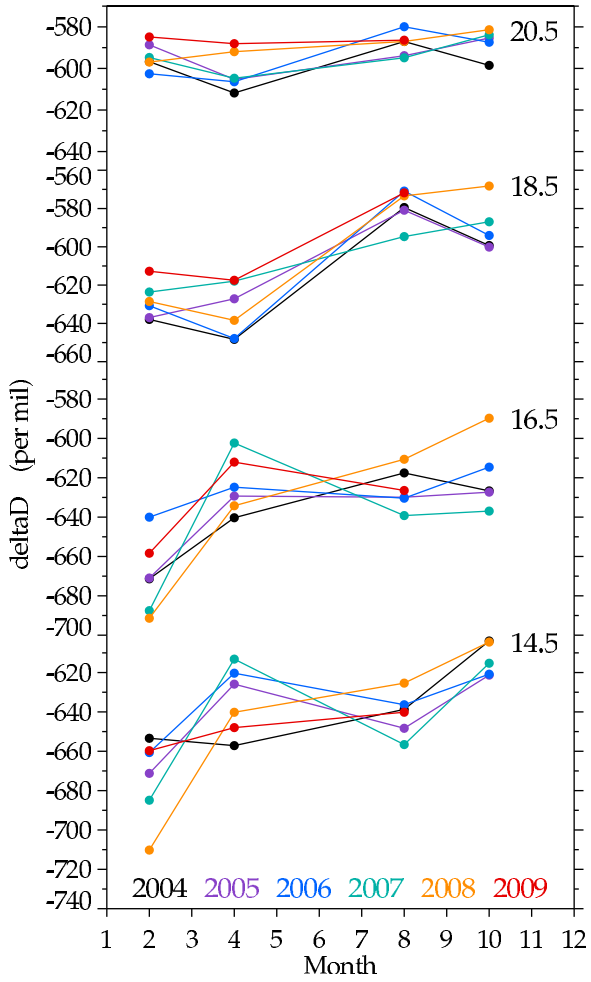

Figure 6. Seasonal variation of δD in the tropics (15°N–15°S) at 14.5, 16.5, 18.5, and 20.5 km. The separate data points denote ACE-FTS measurements during each of the separate years, 2004–2009.

to a regular seasonal cycle could indicate the possible influence of overshooting deep convection [e.g., *Moyer et al.*, 1996; *Dessler and Sherwood*, 2003; *Steinwagner et al.*, 2010]. The climatological vertical profiles of H_2O, HDO and δD in the deep tropics (15°N–15°S) are shown for the four seasons in Figure 5; note that because of the ACE-FTS sampling (Figure 1), these profiles represent measurements during only February, April, August and October. H_2O and HDO exhibit very similar structure and variability, as expected, with minima near and above the cold point tropopause (~17 km), and clear seasonal cycles in minimum values (driest air during February and April, coincident with the coldest tropopause temperatures during these months). The H_2O and HDO minimum values propagate upward from February–April to August and October, consistent with the well-known tape recorder behavior [*Mote et al.*, 1996]. The seasonal profiles of δD however do not show similar behavior. The profiles in Figure 5 do not show evidence of systematic vertical propagation of the minimum originating near 15 km (discussed further below). Near the cold point tropopause (~17 km), δD varies from ~−650‰ in February–April to ~−600‰ in August–October, but above ~20 km there are no substantial differences in δD among seasons.

[12] In the tropical troposphere, in all seasons profiles of δD (Figure 5) show a decrease with height up to a minimum region near 15 km (with values of −625‰ to −675‰), and slight increase with height above this minimum up to approximately 20 km (where δD ~−600‰). This minimum in δD occurs substantially below the cold point tropopause (~17 km), and the corresponding minima in H_2O and HDO. There is a weak but clear seasonality of the magnitude of the minimum δD values near 15 km, with lowest values in February (~−675‰) and higher values (~−650‰ to −625‰) in other seasons. For altitudes 17–20 km δD is less depleted in August and October than in February and April, and we show below that this behavior is linked to influence from NH subtropics. Above 20 km δD shows very little seasonal variability.

[13] Figure 6 shows the δD values for the tropical (15°N–15°S) ACE-FTS measurements (February, April, August, and October) at 14.5, 16.5, 18.5, and 20.5 km for each of the individual years of the ACE-FTS measurements (2004–2009). These yearly time series are constructed from the number of available measurements for each month and year (which varies from ~20 to ~70 for individual months), and much of the year-to-year variability is probably introduced by this sampling. Nonetheless, the results in Figure 6 suggest that the average seasonal variations are robust aspects of δD behavior in the TTL region; for example, the minimum δD observed in February at 14.5 and 16.5 km is observed each individual year, and likewise, the minima during February–April at 18.5 km is observed every year. Note that the seasonal variations do not persist into the overworld stratosphere, with seasonal changes at 20.5 km much smaller than at lower levels.

[14] Further details of tropical seasonality and interannual variability over the ACE-FTS record are highlighted in Figure 7, showing height-time diagrams of H_2O, HDO, and δD over 15°N–15°S; note that these contour diagrams are constructed from measurements occurring four times per year in the tropics (section 2). Figures 7a and 7b show the tape recorder signature in H_2O and HDO, illustrating minimum annual values originating near the tropical tropopause during February and propagating vertically to above 25 km. The patterns are consistent with previous observations of the H_2O tape recorder [*Mote et al.*, 1996; *Randel et al.*, 2001]. There is also a clear signature of the quasi-biennial oscillation (QBO) influence on tropical tropopause temperatures in Figures 7a and 7b, with lower minima of H_2O and HDO near the tropopause during early 2004, 2006 and 2008.

[15] The height-time variability of δD in Figure 7c is substantially different from that of H_2O or HDO. While the lower stratosphere shows some small annual variations, there is no strong evidence for coherent vertical propagation of the annual δD minimum following the H_2O or HDO tape recorder signal (white lines in Figure 7). Seasonal variation in δD is mostly apparent within the TTL (~13–19 km). The relationship between δD and H_2O within the tape recorder region is quantified further in Figure 8, showing a scatter diagram of the individual seasonal (monthly) averages for

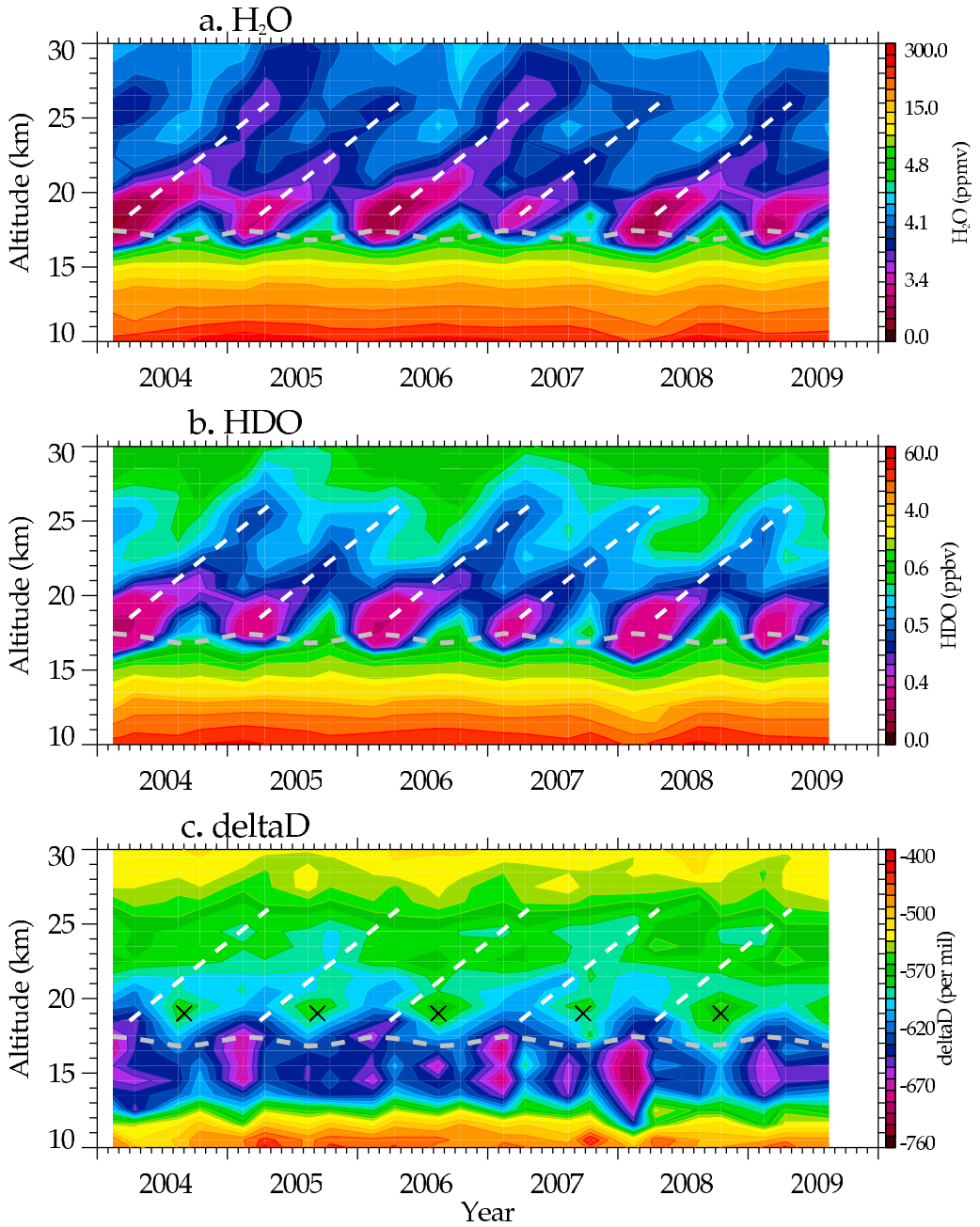

Figure 7. Height-time diagrams of (a) H_2O and (b) HDO mixing ratios, together with (c) δD in the tropics (15°N–15°S) derived from ACE-FTS observations during 2004–2009. These contour diagrams are constructed from the four observations per year in the tropics from the ACE-FTS data (February, April, August, and October). The horizontal white dashed line denotes the tropical cold point tropopause, and the slanted white lines trace the minima in H_2O and HDO originating near the tropopause each year and propagating upward with time (i.e., the "tape recorder"). The white dashed lines in Figure 7c are identical to those in Figures 7a and 7b and trace the H_2O tape recorder. The crosses in Figure 7c denote relative minima above the tropopause associated with the NH summer monsoon signal (as discussed in text).

each year for altitudes 17–25 km (using the same data as in Figure 6). In this diagnostic a coherent tape recorder signal in δD should exhibit a compact relationship with H_2O; results in Figure 8 show correlation between δD and H_2O at levels closest to the tropopause (17.5–18.5 km), but no compact relationship over higher altitudes. This behavior is consistent with the lack of an obvious tape recorder signal in Figure 7c, and lack of any significant seasonal variation in δD above 20 km in Figure 5.

[16] One additional annually repeating feature appears in the tropical δD patterns in Figure 7c that is not apparently linked to upward propagation of signals from the tropopause, namely a maximum centered near 19 km occurring during each August and October (marked with crosses). This

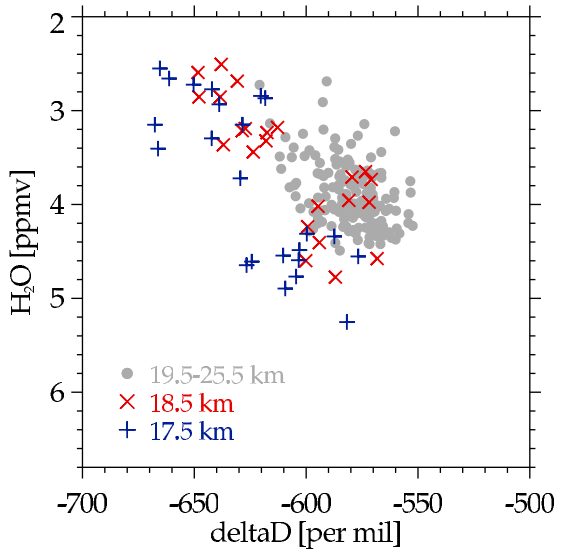

Figure 8. Scatter diagram of H_2O versus δD for ACE-FTS measurements in the tropics (15°N–15°S) over individual altitudes 17.5–25.5 km (crosses indicate levels closest to the tropopause, as indicated). Each point represents a monthly average (February, April, August, October), and these are the same data contoured in Figure 7.

localized maximum above the tropopause is also evident in the August and October profiles in Figure 4. This maximum occurs for each year of data (see also the 18.5 km time series in Figure 5), and is related to propagation from higher northern latitudes of enhanced δD during the NH summer monsoon seasons (as discussed further below).

3.3. Correction for Methane Oxidation

[17] To more clearly characterize water isotopologue behavior in the stratosphere, it is necessary to correct the H_2O and HDO measurements to remove the effects of methane oxidation. Methane (CH_4) oxidation is an important source of stratospheric water vapor, and because atmospheric methane is heavier in isotopic composition than near-tropopause water, acts as a source of heavy water in the stratosphere [e.g., *Zahn et al.*, 2006]. In the process of methane oxidation the total amount of stratospheric hydrogen is conserved, i.e., $(H_2 + H_2O + 2CH_4)$ = constant (where H_2 is molecular hydrogen). If $H_2 \sim$ constant, then $(H_2O + 2CH_4) \sim$ constant; more generally, modeling and observational studies have suggested a relationship $(H_2O + \beta CH_4)$ = constant. Hence the contribution to H_2O increase from CH_4 oxidation can be calculated from observations of stratospheric CH_4, i.e., $\Delta H_2O = -\beta(CH_4 - CH_{4entry})$, where CH_{4entry} is the value of CH_4 of air near the tropical tropopause. Model calculations [*le Texier et al.*, 1988] suggest a range of β varying from ~1.8 to 2.2. *Dessler et al.* [1994] have calculated $\beta = 1.94 \pm 0.27$ from aircraft measurements in the lower stratosphere, and *Remsberg et al.* [1996] and *Wrotny et al.* [2010] find β can range from ~1.6 to 2.6 in the middle and upper stratosphere on the basis of satellite data. Here we use a value of $\beta = 2.0$, and also test the sensitivity of varying β over 1.8–2.2.

[18] The oxidation of CH_3D likewise results in the production of HDO, wherein deuterium is conserved, i.e., (HD + HDO + CH_3D) = constant. Changes in HDO can then be calculated from changes in HD and CH_3D. In this work we use ACE-FTS observations of CH_4 and estimate changes in HD and CH_3D following *McCarthy et al.* [2004]: $\Delta HDO = -\Delta HD - \Delta CH_3D = (0.63 \times 10^{-4} - 5.16 \times 10^{-4})\ \Delta CH_4 = -4.53 \times 10^{-4}\ (CH_4 - CH_{4entry})$. We calculate values of ΔH_2O and ΔHDO as a function of CH_4 in the stratosphere, using seasonal ACE-FTS observations of CH_4; these calculations use a mean entry value of CH_{4entry} = 1.75 ppbv. These values are then subtracted from the stratospheric H_2O and HDO fields to approximately remove the methane contributions and δD is recalculated to provide methane corrected values.

[19] Application of the methane correction (Figure 9) results in much less variation in δD throughout the stratosphere compared to Figure 3, namely the overall increase in δD with altitude and latitude seen in Figure 3 is removed by the methane correction. Results in Figure 8 focus on the latitude band 60°N–60°S to avoid the region of the Antarctic polar vortex and the associated dehydration region (south of 60°S during JJA and SON). There is still a relative minimum in δD near the tropopause in both the tropics and extratropics. The overall value of δD in the stratosphere in Figure 9 is ~600‰ ± 18‰, close to the value at the top of the TTL (consistent with this being an approximate stratospheric entry value for δD at the top of the TTL). The stratospheric average values change only slightly if different values of β ($\Delta H_2O/\Delta CH_4$ ratio) are used: $\beta = 1.8$ results in −606‰ ± 15‰, and $\beta = 2.2$ gives −591‰ ± 21‰. We note that these ACE-FTS values for the isotopic composition of water entering the stratosphere are intermediate between values previously reported from satellite measurements (−670‰ ± 80‰ by *Moyer et al.* [1996], −676‰ ± 20‰ by *Johnson et al.* [2001], and −653‰ ± 25‰ by *McCarthy et al.* [2004]) and those from some localized aircraft measurements (−400‰ to −600‰ by *Hanisco et al.* [2007] and *Sayres et al.* [2010]). Given expected uncertainties, the measurements presented here could be consistent with any of these. The differences are a useful caution about possible systematics in any or all of these measurements, but we note that the spatial and temporal variability, as we focus on in this work, is unlikely to be affected significantly, and the conclusions drawn from this variability are more robust than inferences that would depend on a precise value for δD.

[20] The one stratospheric feature that now stands out in the methane-corrected Figure 9 is a systematic enrichment in the NH lower stratosphere during JJA and SON (up to about 20 km, or 500 K potential temperature). This δD enhancement is associated with the NH summer monsoon circulations, especially that over North America, as shown below. This pattern persists seasonally through SON (and slightly into DJF), and during JJA and SON the maximum extends into tropical latitudes near 18–20 km, accounting for the periodic tropical isotopic enhancements near these altitudes seen in Figure 7c and in the tropical averages in Figure 5 (the August and October high values near 18.5 km). Note that this maximum is evident each individual year in Figure 7c (and Figure 6), demonstrating that it is a robust climatological feature. This monsoon effect accounts for a systematic NH-SH asymmetry in δD in the lower stratosphere during the NH summer and autumn seasons. This asymmetry is evident on close inspection of the uncorrected δD in

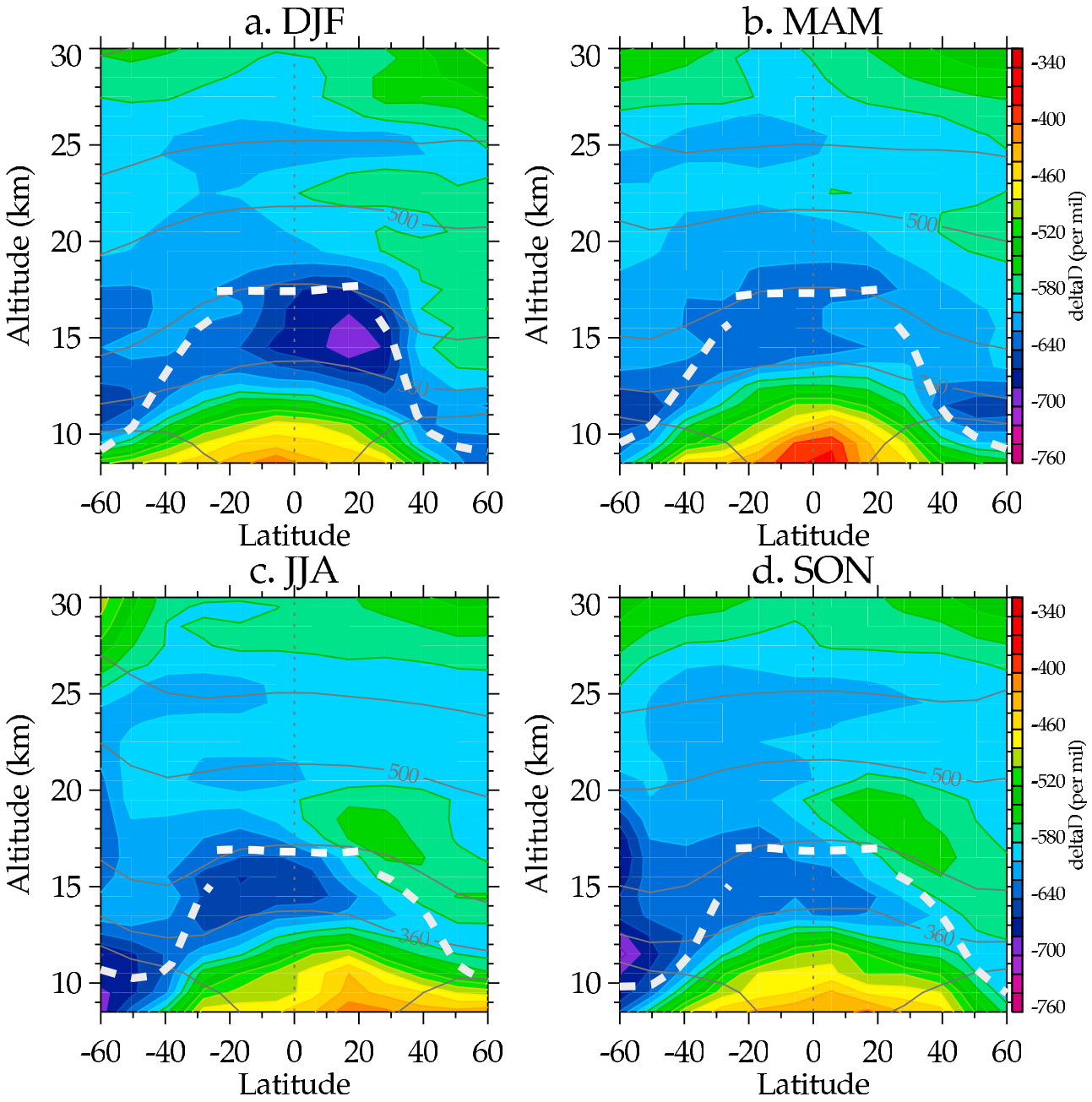

Figure 9. Meridional cross sections of δD for each season, with corrections applied to remove methane effects. The white dashed line denotes the tropopause. Results are restricted to the latitude band 60°N–60°S to avoid the region of the Antarctic polar vortex and the associated dehydration region (south of 60°S during June–August (JJA) and September–November).

Figure 3, but is more clearly highlighted in the methane corrected results in Figure 9. As a note, previous modeling and trajectory studies [*Bannister et al.*, 2004; *Gettelman et al.*, 2004; *Lelieveld et al.*, 2007; *Wright et al.*, 2011] have identified transport from the NH summer monsoons into the tropics as a potentially important mechanism contributing to the moist phase of the water vapor tape recorder (e.g., the moist phases; see Figures 7a and 7b). This transport from the NH monsoon regions is less evident in the H_2O and HDO fields directly, because latitudinal gradients between the deep tropics and monsoon regions are relatively small; in contrast, latitudinal gradients in δD are substantially larger, so that transport from the monsoon regions appears more evident in δD (e.g., the JJA and SON patterns in Figure 9).

3.4. Latitude-Longitude Structure

[21] To more clearly understand the role of convection we examine the zonal variation of water isotopic composition. The isotopic features described above, a seasonally migrating isotopic minimum centered near 15 km that appears unconnected to water vapor changes and a seasonal isotopic enhancement above the tropopause that appears unconnected

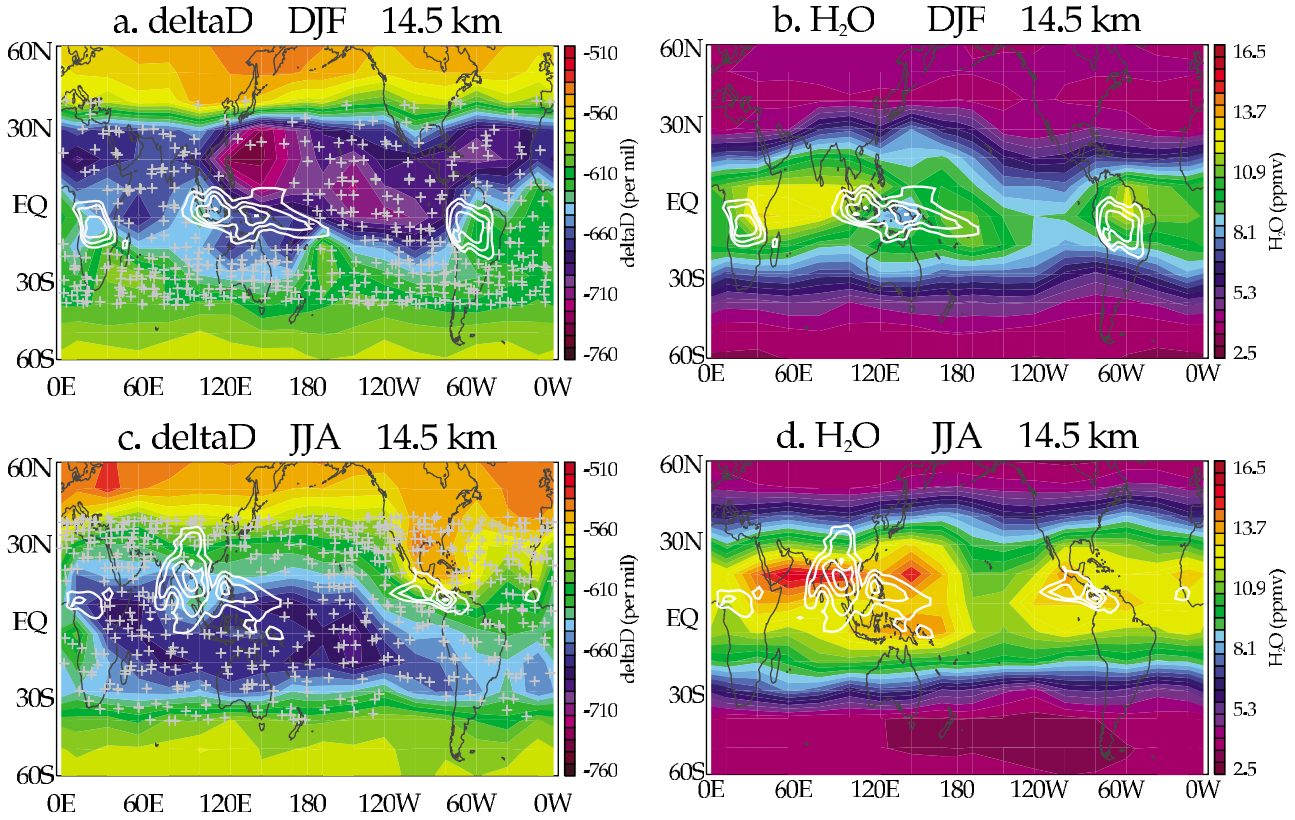

Figure 10. Combined ACE-FTS measurements from all years (2004–2009) gridded onto 10° latitude by 20° longitude bins. (left) Latitude-longitude sections of δD at 14.5 km for Northern Hemisphere winter (December–February) and summer (JJA) seasons. Crosses indicate the locations of the ACE-FTS observations for these seasons (only shown over 40°N–40°S). (right) The corresponding H_2O mixing ratios at this altitude. The white contours denote the regions of strongest climatological deep convection, as measured by outgoing longwave radiation (contours of 220, 210, 200, and 190 K).

to tropopause temperatures, were diagnosed from zonally averaged data but also have zonal structure. As described in section 2, the ACE-FTS measurements from all years (2004–2009) are combined and gridded onto 10° latitude by 20° longitude bins, to reveal climatological regional structure. Because ACE-FTS observations are available only down to cloud top, there are few measurements available at altitudes below ~12–14 km over regions of chronic deep convection. At altitudes within the UTLS, there is little influence of methane oxidation, so we primarily focus on uncorrected δD values.

[22] The influence of convection is suggested by the regional climatological structures of δD and corresponding fields of H_2O within the TTL region (see Figure 10 for solstice seasons at 14.5 km). Figure 11 shows δD for all four seasons at 16.5 km. Regions of chronic deep tropical convection are marked on the basis of climatological outgoing longwave radiation (OLR) [*Liebmann and Smith*, 1996] values less than 220 K; these highlight the well-known regions of deep convection over Africa, Indonesia, and South America during DJF and over Africa, SE Asia, and Central America during JJA. There are few ACE-FTS measurements directly over climatological deep convection, however, so the spatial patterns of δD result mainly from interpolating nearby measurements. The locations of the corresponding tropical ACE-FTS observations for each season are marked in the δD plots in Figure 10. The tropical upper troposphere is both wetter and isotopically lighter (higher H_2O and lower δD) than the extratropics at these altitudes (where air lies above the local tropopause and so reflects stratospheric values). Within the tropics, deep convection is associated with enhanced water vapor but not with enhancement in δD. Instead the lowest regional δD values lie near the same longitude band as the strongest convection (over the western and central Pacific ocean in DJF and over the Indian and Pacific oceans in JJA). The correlation is strongest in DJF, when the gridded results suggest the minimum δD values are located north of the strongest Indonesian convection, but the detailed structure should be viewed cautiously given the limited ACE-FTS sampling in this region. In JJA, minimum δD occurs over a broad region of the Indian and Pacific oceans, centered to the south of the strongest convection over SE Asia. The minimum δD values in DJF in Figure 10 are substantially lower than those in JJA (or other seasons), and this region is the primary origin of the seasonal variation in zonal mean isotopic composition discussed above (i.e., Figures 3, 5, and 6).

[23] Near the tropical tropopause (Figure 11), the isotopic effects of convection are less consistent, and appear to have opposite sign in different regions and times. Again, the seasonal minimum of lowest tropical values during DJF is evident, and in all seasons the lowest values of δD (enhanced

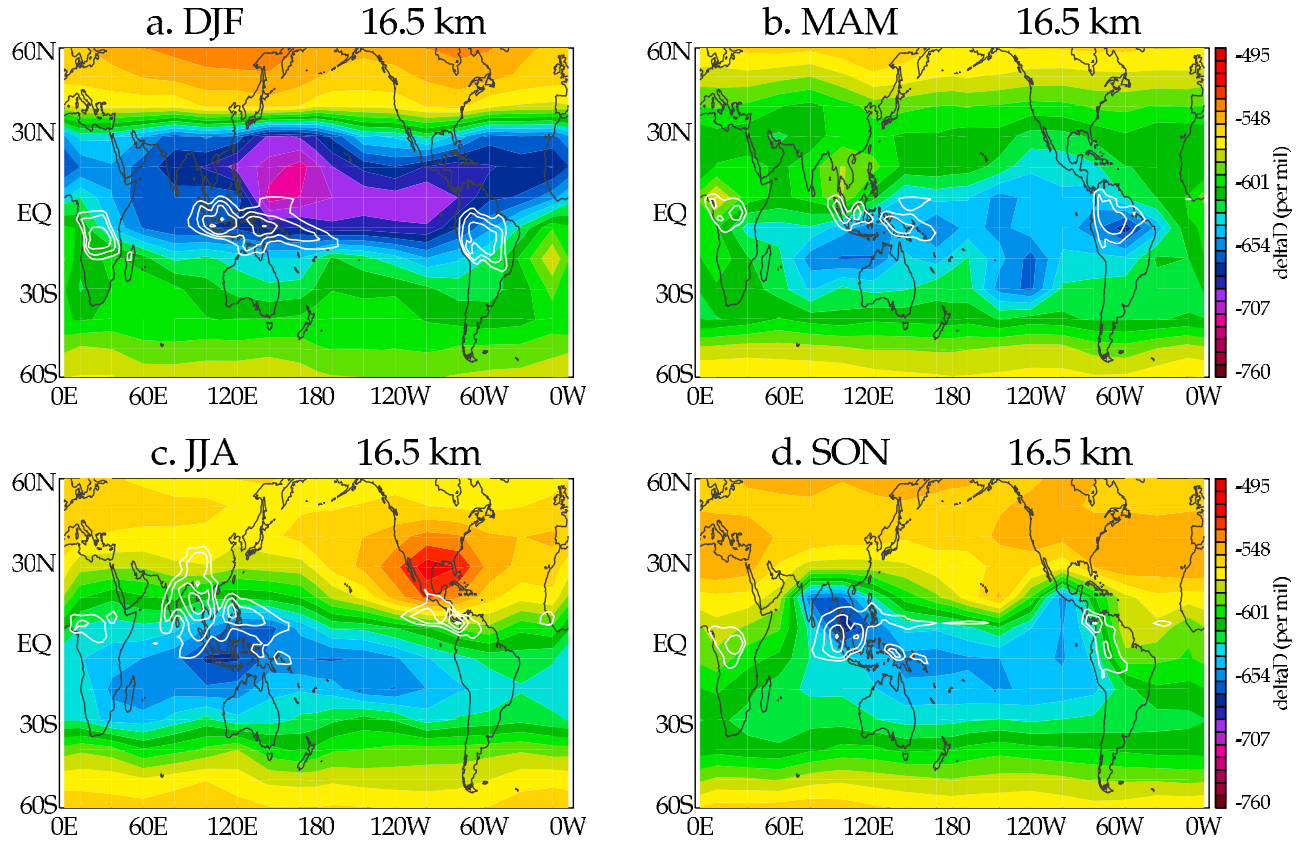

Figure 11. Cross sections of δD at 16.5 km for each of the four seasons, with data treatment as in Figure 10. White contours denote the strongest climatological tropical convection.

depletion) are observed near the longitude regions of deep convection in the western Pacific, Indian Ocean, and southeast Asia. Minimum δD in DJF occur somewhat north of the strongest Indonesian convection, and the JJA patterns have a symmetric spatial structure with δD minima southward of the strongest convection over SE Asia. In both cases, these minima are downstream of the cross-equatorial Hadley circulation tied to the seasonal convection maxima. That these isotopic features are driven by convective influence is suggested by the fact that patterns of δD minima in DJF and JJA are not centered over the equator, as might be expected if these minima were primarily tied to the minimum temperatures near the tropical cold point tropopause, which are more symmetric [e.g., *Fueglistaler et al.*, 2009]. While the western Pacific–Asian convection is associated with isotopic minima at tropopause level, the strong summer convection over the North American region appears associated with isotopic perturbations of opposite sign (Figure 11). The strong localized maximum values of δD over North America (NA) are in fact the dominant isotopic feature at this level in JJA. Figure 12 shows this δD behavior in conjunction with the corresponding structure of H_2O. Although water exhibits similarly sized maxima over both the NA and SE Asian monsoons, the isotopic signatures are quite different, and these results highlight a systematic difference in the isotope behavior between the NA and Asian monsoon circulations.

[24] The differing isotopic signatures may seem surprising because in many respects the Asian monsoon has a more vigorous circulation than the NA counterpart, and has a more substantial influence on chemical constituents in the UTLS [e.g., *Park et al.*, 2007; *Randel et al.*, 2010]. But the background thermodynamic structure in the regions is quite different, as mentioned by *Dessler and Sherwood* [2003] and *Dessler et al.* [2007], and results in differences in relative humidity that can affect the convective ice evaporation, as discussed further below. Figure 13a shows vertical profiles of δD over the NA and Asian monsoon regions for each individual year of the ACE-FTS observations, highlighting the strong enhancements over NA for ~15–18 km, clear differences with the Asian region, and highly repeatable observations for each individual year. Figure 13b shows the same results but using H_2O as a vertical coordinate, demonstrating that the differences in δD over ~14–18 km reflect isotopic enrichment over North America, as would be expected from the addition of convective ice, and not simply differing amounts of H_2O. These monsoonal patterns in δD persist in the lower stratosphere into NH autumn (SON and partly into DJF), and the signal vanishes by the following NH spring (MAM; see Figure 11), presumably because of "flushing" of the extratropical lower stratosphere [e.g., *Bönisch et al.*, 2009]. This monsoon influence imparts a systematic NH-SH asymmetry in δD to the lower stratosphere (as seen in Figure 9) that extends into tropical latitudes.

4. Summary and Discussions

[25] As noted in the Introduction, the HDO/H_2O ratio contains information on convective transport within the

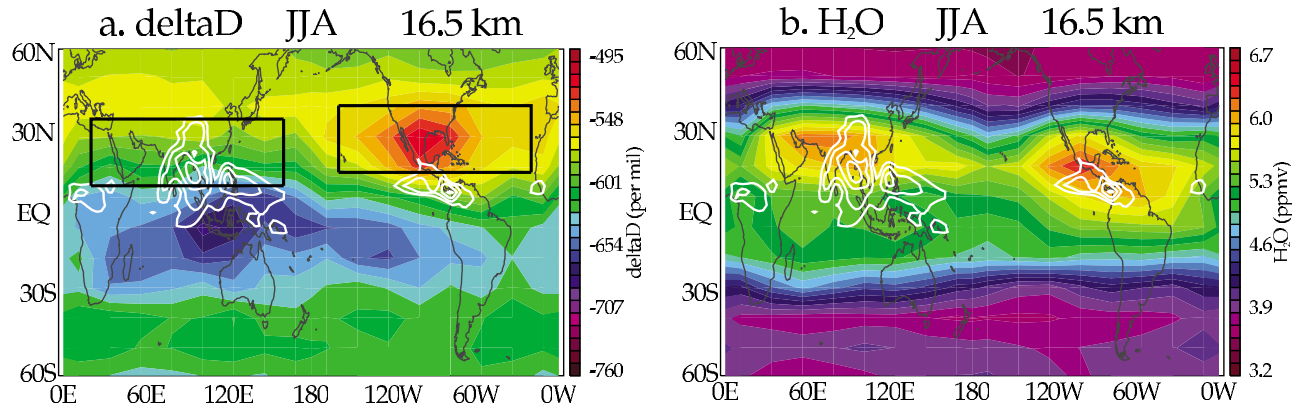

Figure 12. Cross sections of (a) δD and (b) H_2O at 16.5 km during JJA. The δD field has been corrected for methane effects, although this effect is small and only influences the highest latitudes. White contours denote strongest climatological tropical convection, and the black boxes denote the averaging regions for Figures 13 and 14. Note the isotopic enrichment correlated with high water vapor over the North American (NA) monsoon but the lack of a similar signal over the SE Asian monsoon region.

UTLS region, and previous observations (from aircraft and satellite data) have revealed various aspects of this behavior. The long record of high-quality ACE-FTS data provides the opportunity to resolve the climatological seasonal behavior of δD on a global scale, including regional (latitude-longitude) structure. The key features revealed by these data include the detailed behavior of the tropical seasonal cycle (and links to deep convection), and the differential isotopic effects of convection in different locations, including aspects of the NH summer monsoon circulations. These are discussed in turn below.

[26] Consistent with previous observations, the overall vertical structure of δD in the tropics exhibits a minimum near 15 km in each season ($\sim$−675‰ to −625‰), with a small increase above this level to $\sim$20 km ($\sim$−600‰), and more or less constant values in the stratosphere above (after correction for methane effects). The climatological tropical minimum near 15 km is situated below the cold point tropopause ($\sim$17 km), and on this aspect the ACE-FTS data are in good agreement with the aircraft measurements of *Hanisco et al.* [2007] and MIPAS satellite observations [*Payne et al.*, 2007]. This behavior was not found in the limited ATMOS satellite observations of *Kuang et al.* [2003], but it should be noted that these data include only 11 profiles over the NH subtropics ($\sim$10°–20°N) during November 1994. The observed tropical minimum in δD near 15 km and increase into the lower stratosphere is a potential consequence of evaporation of ice lofted in deep convection. Similar features have been reproduced in the idealized simulations of *Dessler et al.* [2007] and *Read et al.* [2008], in mesoscale numerical simulations of *Blossey et al.* [2010], and general circulation model simulations of *Schmidt et al.* [2005]. The in-mixing of air from extratropics [e.g., *Konopka et al.*, 2009; *Ploeger et al.*, 2010] is an

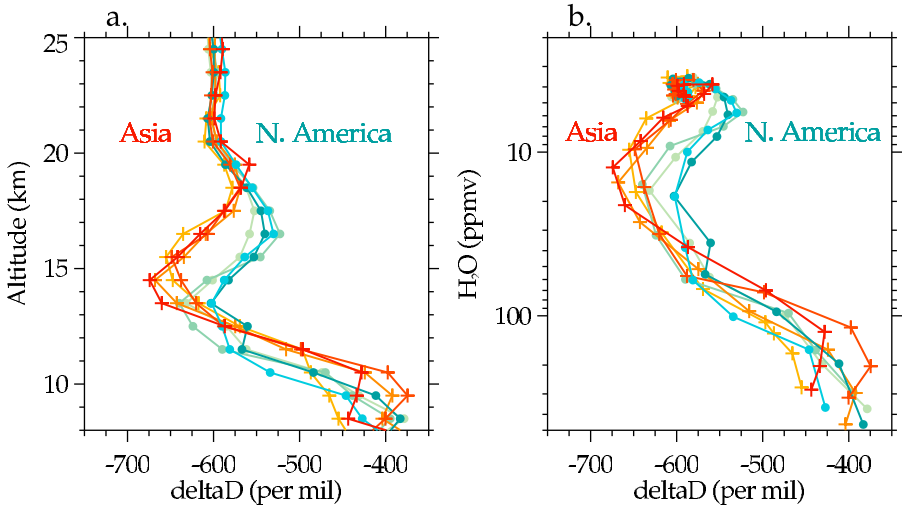

Figure 13. Vertical profiles of δD from ACE-FTS observations over the NA and Asian monsoon regions (black boxes in Figure 12). Each of the curves shows measurements from individual years, when there are adequate observations within the respective regions. Figure 13a shows the results in altitude coordinates, and Figure 13b shows δD as a function of water vapor.

additional mechanism for enhancing the HDO/H_2O ratios in the tropical lower stratosphere; such in-mixing from the NH seems especially clear in the methane-corrected δD values during JJA and SON in Figure 9. This relative enhancement stands in contrast to the extremely depleted δD values observed in the Antarctic upper troposphere (Figure 4a). Presumably the near-Rayleigh Antarctic upper troposphere reflects an absence of the convective ice lofting and/or in-mixing effects that provide isotopic enhancement in the tropical UTLS and that in turn influence the entire stratosphere.

[27] The limited tropical sampling of ACE-FTS data (4 months per year) reveal seasonal variation in δD in the TTL, including the tropical minimum values near 15 km, with the strongest depletion (lowest δD) during February. This behavior is observed during each year of the ACE-FTS measurements (Figure 5). The spatial structure of this minimum appears linked to the region of strongest climatological convection over Indonesia, although it is located not directly over the convection but toward the winter hemisphere (Figures 10–11). This spatial structure is evident up to the level of the tropical tropopause (i.e., spanning the TTL), and a mirror image pattern at tropopause level is observed during NH summer (JJA Figure 11). δD therefore exhibits a minimum in the subtropical upper troposphere, centered toward the winter hemisphere in solstice seasons (and more nearly over the equator at the equinoxes). This seasonal behavior is consistent with the aircraft δD observations in NH subtropics reported by *Sayres et al.* [2010], namely, a pronounced minimum near 15 km during NH winter but not during summer. The mechanism for shifting the δD minima toward the winter hemisphere during solstice seasons is not understood, but could be related to the associated cross-equatorial Hadley circulation tied to the convection. The stronger minimum observed during DJF imparts an overall annual cycle in the tropics that extends to tropopause level or slightly above, but appears not to propagate upward. The seasonal cycle in minimum δD values is another feature that is not well understood, but could be linked to the stronger deep convection to higher altitudes over Indonesia during NH winter [e.g., *Zhang*, 1993; *Chae and Sherwood*, 2010]. The spatial patterns observed in ACE-FTS data suggest the dominant influence of deep convection for determining minimum values of δD in the TTL, rather than tropical tropopause temperatures, which would presumably impart an equatorially symmetric structure (because tropical tropopause minimum temperatures are centered over the equator [e.g., *Fueglistaler et al.*, 2009]).

[28] The tropical observations available with ACE-FTS show clear evidence for the tropical tape recorder in H_2O and HDO (Figures 7a and 7b). However, the ACE-FTS data do not show evidence for a corresponding systematic variation in δD correlated with this tape recorder (Figure 7c), or a corresponding compact relationship between δD and H_2O in the tropical lower stratosphere (Figure 8). This lack of an obvious tape recorder signal in δD is surprising, given that the annual cycle in tropical tropopause temperature is expected to impart a variation of ~70‰ in δD simply because of Rayleigh fractionation. This amount of variability near the tropopause is evident in the ACE-FTS data (Figure 8), although there is almost zero coherent seasonal variation above 20 km (Figure 5). The lack of a coherent vertical propagation of the δD signal near the tropopause is one of the more curious and poorly understood aspects of the ACE-FTS results. Because the tape recorder is clearly observed up to ~28 km in H_2O and HDO, poor temporal sampling is not likely a cause of the lack of a signal in δD. For altitudes just above the tropical tropopause, much of the annual variation in δD originates from horizontal transport from the NH during JJA and SON (Figures 7 and 9), originating in the NH summer monsoons (Figure 11). This transport reaches the tropical lower stratosphere but is not apparently entrained in a coherent manner into the tropical upwelling circulation (according to Figure 9); this aspect is poorly understood but could be partly due to the weak upwelling during NH summer (near-stagnant conditions according to *Yang et al.* [2008]).

[29] *Steinwagner et al.* [2010] have reported a coherent tape recorder signal in δD derived from 19 months of MIPAS data (during 2002–2004), with a magnitude just above the tropopause of ~100‰; they propose that the enhanced amplitude (above Rayleigh fractionation) results from overshooting convection. It is unclear how to reconcile the lack of a coherent tape recorder signal in the ACE-FTS results with the MIPAS observations reported by *Steinwagner et al.* [2010], although we note a very different sampling between the two sets of observations (MIPAS HDO data has much coarser vertical resolution (~6–8 km) than does ACE-FTS (~3 km), but greater temporal sampling). One factor that can possibly confuse a tape recorder signal in δD is the localized δD maximum in tropical latitudes over ~18–20 km during NH summer (JJA) and autumn (SON) (Figures 7 and 9), associated with transport from the NH summer monsoon regions. A similarly timed maximum was observed by *Steinwagner et al.* [2010, Figure 2], but not well resolved in altitude because of the relatively low resolution of the MIPAS retrieval. It is possible that this monsoon influence could be confused with tropical tropopause δD variations in lower-resolution data (such as MIPAS), so that the influence of tropical convective overshooting could be overestimated.

[30] The ACE-FTS data show a regional isotopic enrichment in the lower stratosphere during NH summer, with a local maximum apparently linked to the North American summer monsoon (Figure 12). This is likely a result of deep convective overshooting into the lower stratosphere, akin to aircraft observations of isotopic enhancements associated with deep convective remnants over this region [*Hanisco et al.*, 2007]. The strong enrichment of δD at 16.5 km in the North American monsoon region compared to a smaller δD signature over the Asian monsoon region (Figure 12) is somewhat surprising, particularly since other tracers (such as CO or HCN) indicate a stronger signature of transport within the Asian monsoon compared to the NA monsoon [e.g., *Park et al.*, 2007; *Randel et al.*, 2010]. However, one possible explanation for this difference in behavior is that the influence of convection on water vapor isotopes is likely linked to both the depth and intensity of convection and the background thermodynamic structure [*Dessler and Sherwood*, 2003]. In particular, if the UTLS is near ice saturation, then much of the ice detrained from deep convection above the tropopause will precipitate out and not produce an enriched δD signature. In contrast, if convection

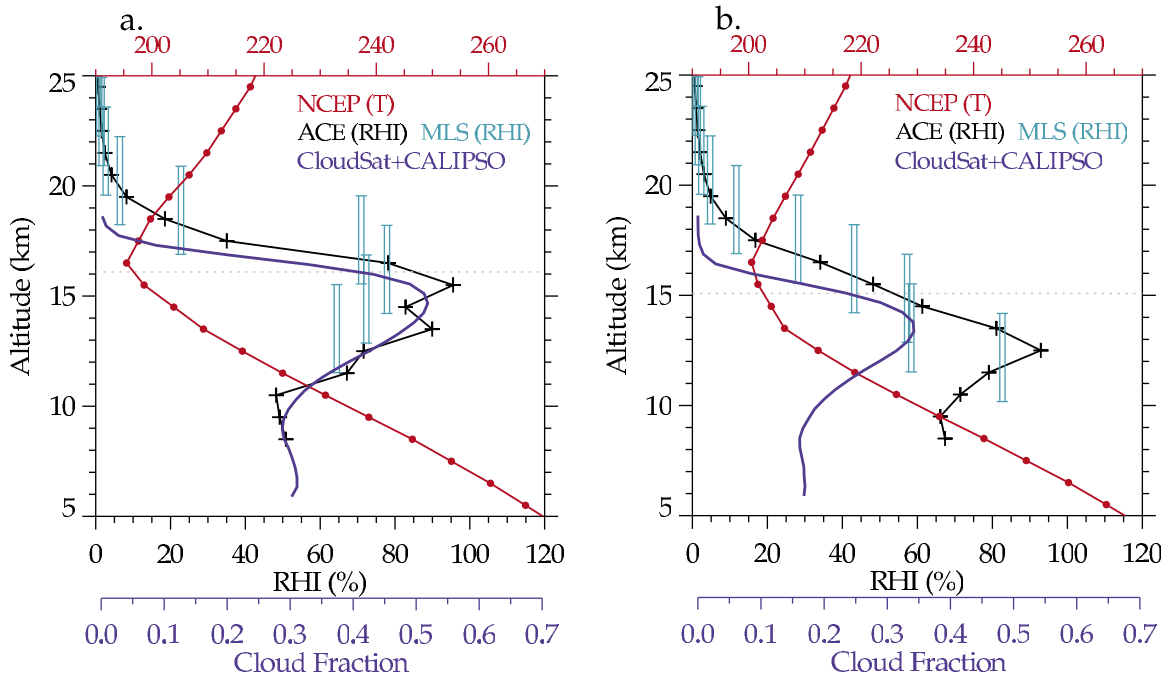

Figure 14. Vertical profiles of climatological thermodynamic and cloud fraction statistics over the (a) Asian and (b) NA monsoon regions (with areas defined by the black boxes in Figure 12). Red lines show the temperature profile, with the dashed horizontal line indicating the tropopause. Relative humidity is shown as calculated from ACE-FTS and Aura MLS data, showing reasonable agreement. Solid blue lines show cloud fraction statistics derived from CloudSat + CALIPSO observations.

detrains ice into subsaturated air, then sublimation can occur rapidly, resulting in enriched δD at higher altitudes.

[31] The background thermodynamic structure over the Asian and North American monsoon regions during summertime shows differences that could lead to the differing isotopic effects (Figure 14). The regions differ in aspects including temperature and tropopause height, relative humidity with respect to ice (calculated from both ACE-FTS and MLS data), and cloud occurrence frequency (from CloudSat [*Stephens et al.*, 2008] and CALIOP [*Winker et al.*, 2007] satellite observations). The tropopause is somewhat lower and the uppermost troposphere is considerably drier in the North American monsoon compared to the Asian monsoon (mean relative humidity near the tropopause is ~80% over Asia versus ~50% over North America). This background structure is consistent with the potential for greater release of enriched δD from convective detrainment in the North American monsoon.

[32] There are several caveats to interpretation of the enhanced δD and background thermodynamic structure associated with the North American monsoon. The maximum δD enhancement in Figure 12 is north of the region over central America where the strongest convection is indicated by the OLR statistics. Yet, it is known that some of the strongest convection on the planet occurs during the NA monsoon over the south central United States, and there is evidence of convective systems extending deep into the stratosphere in this region [*Wang*, 2003, *Hanisco et al.*, 2007]. Note that convection detraining into relatively dry air in the upper troposphere or lower stratosphere will produce little or no anvil because the cloud ice will sublimate rapidly as dry air is entrained. Hence, such convection will not produce significant cloud frequency apparent in products such as OLR, CloudSat, or CALIOP. Nevertheless, these convective systems could significantly enrich the isotopic composition of water vapor in the lowermost stratosphere.

[33] In summary, the ACE-FTS data provide a novel perspective on the global climatological behavior of HDO and HDO/H_2O ratios, and highlight a significant amount of spatial structure to the observed seasonal variability. It is likely there is also a high degree of temporal variability in these quantities tied to the transient nature of deep convection, although this is poorly sampled by ACE-FTS. The observed regional patterns (especially the North American summer monsoon) suggest that the background thermodynamic structure is important for understanding δD behavior (as noted by *Dessler and Sherwood* [2003]), in addition to details of the convection. This behavior significantly complicates interpretation of δD as a diagnostic for UTLS convective processes. Several open questions remain regarding the large-scale seasonal structure observed in the ACE-FTS results: (1) What is the origin of the apparent seasonal cycle in the tropical δD minimum near 15 km (which is minimally sampled by ACE-FTS)? (2) Why does the tropical δD minimum shift toward the winter hemisphere (and is this an artifact of the ACE-FTS sampling outside of convection)? (3) How does the tropopause-level seasonal variation in δD couple with transport from the NH summer monsoons, so that seasonal signals do not appear to propagate upward in the tropical stratosphere? Further observational and modeling studies will be required to improve characterization and understanding of these behaviors.

[34] **Acknowledgments.** We thank Chuck Bardeen, Rolando Garcia, Andrew Gettelman, Chuntao Liu, and Holger Vömel for discussions and comments on the manuscript and three reviewers for constructive comments that improved the paper. This work was partially supported under the NASA Aura Science Program. ACE is funded primarily by the Canadian Space Agency. The National Center for Atmospheric Research is operated by the University Corporation for Atmospheric Research, under sponsorship of the National Science Foundation.

References

Bannister, R. N., A. O'Neill, A. R. Gregory, and K. M. Nissen (2004), The role of the South-east Asian monsoon and other seasonal features in creating the 'tape recorder' signal in the unified model, *Q. J. R. Meteorol. Soc.*, *130*, 1531–1554, doi:10.1256/qj.03.106.

Bernath, P. F., et al. (2005), Atmospheric Chemistry Experiment (ACE): Mission overview, *Geophys. Res. Lett.*, *32*, L15S01, doi:10.1029/2005GL022386.

Blossey, P. N., Z. Kuang, and D. M. Romps (2010), Isotopic composition of water in the tropical tropopause layer in cloud-resolving simulations of an idealized tropical circulation, *J. Geophys. Res.*, *115*, D24309, doi:10.1029/2010JD014554.

Bönisch, H., A. Engel, J. Curtius, T. Birner, and P. Hoor (2009), Quantifying transport into the lowermost stratosphere using simultaneous in-situ measurements of SF6 and CO_2, *Atmos. Chem. Phys.*, *9*(16), 5905–5919, doi:10.5194/acp-9-5905-2009.

Boone, C. D., R. Nassar, K. A. Walker, Y. Rochon, S. D. McLeod, C. P. Rinsland, and P. F. Bernath (2005), Retrievals for the atmospheric chemistry experiment Fourier transform spectrometer, *Appl. Opt.*, *44*, 7218–7231, doi:10.1364/AO.44.007218.

Carleer M. R., et al. (2008), Validation of water vapour profiles from the Atmospheric Chemistry Experiment (ACE), *Atmos. Chem. Phys. Discuss.*, *8*, 4499–4559, doi:10.5194/acpd-8-4499-2008.

Chae, J. H., and S. Sherwood (2010), Insights into cloud-top height and dynamics from the seasonal cycle of cloud-top heights observed by MISR in the west Pacific region, *J. Atmos. Sci.*, *67*, 248–261, doi:10.1175/2009JAS3099.1.

Coffey, M. T., J. W. Hannigan, and A. Goldman (2006), Observations of upper tropospheric/lower stratospheric water vapor and its isotopes, *J. Geophys. Res.*, *111*, D14313, doi:10.1029/2005JD006093.

Dessler, A. E., and S. C. Sherwood (2003), A model of HDO in the tropical tropopause layer, *Atmos. Chem. Phys.*, *3*, 2173–2181, doi:10.5194/acp-3-2173-2003.

Dessler, A. E., E. M. Weinstock, E. J. Hintsa, J. G. Anderson, C. R. Webster, R. D. May, J. W. Elkins, and G. S. Dutton (1994), An examination of the total hydrogen budget of the lower stratosphere, *Geophys. Res. Lett.*, *21*, 2563–2566, doi:10.1029/94GL02283.

Dessler, A. E., T. F. Hanisco, and S. Fueglistaler (2007), Effects of convective ice lofting on H_2O and HDO in the tropical tropopause layer, *J. Geophys. Res.*, *112*, D18309, doi:10.1029/2007JD008609.

Fueglistaler, S., A. E. Dessler, T. J. Dunkerton, I. Folkins, Q. Fu, and P. W. Mote (2009), Tropical tropopause layer, *Rev. Geophys.*, *47*, RG1004, doi:10.1029/2008RG000267.

Gettelman, A., D. E. Kinnison, T. J. Dunkerton, and G. P. Brasseur (2004), Impact of monsoon circulations on the upper troposphere and lower stratosphere, *J. Geophys. Res.*, *109*, D22101, doi:10.1029/2004JD004878.

Hanisco, T. F., et al. (2007), Observations of deep convective influence on stratospheric water vapor and its isotopic composition, *Geophys. Res. Lett.*, *34*, L04814, doi:10.1029/2006GL027899.

Hegglin, M. I., et al. (2008), Validation of ACE-FTS satellite data in the upper troposphere/lower stratosphere (UTLS) using non-coincident measurements, *Atmos. Chem. Phys.*, *8*, 1483–1499, doi:10.5194/acp-8-1483-2008.

Johnson, D. G., K. W. Jucks, W. A. Traub, and K. V. Chance (2001), Isotopic composition of stratospheric water vapor: Measurements and photochemistry, *J. Geophys. Res.*, *106*(D11), 12,211–12,217, doi:10.1029/2000JD900763.

Konopka, P., J.-U. Grooß, F. Plöger, and R. Müller (2009), Annual cycle of horizontal in-mixing into the lower tropical stratosphere, *J. Geophys. Res.*, *114*, D19111, doi:10.1029/2009JD011955.

Kuang, Z., G. C. Toon, P. O. Wennberg, and Y. L. Yung (2003), Measured HDO/H_2O ratios across the tropical tropopause, *Geophys. Res. Lett.*, *30*(7), 1372, doi:10.1029/2003GL017023.

Lelieveld, J., et al. (2007), Stratospheric dryness: Model simulations and satellite observations, *Atmos. Chem. Phys.*, *7*, 1313–1332, doi:10.5194/acp-7-1313-2007.

le Texier, H., S. Solomon, and R. R. Garcia (1988), The role of molecular hydrogen and methane oxidation in the water vapor budget of the stratosphere, *Q. J. R. Meteorol. Soc.*, *114*, 281–295, doi:10.1002/qj.49711448002.

Liebmann, B., and C. A. Smith (1996), Description of a complete (interpolated) outgoing longwave radiation dataset, *Bull. Am. Meteorol. Soc.*, *77*, 1275–1277.

Lossow, S., et al. (2011), Comparison of HDO measurements from Envisat/MIPAS with observations by Odin/SMR and SCISAT/ACE-FTS, *Atmos. Meas. Tech.*, *4*, 1855–1874, doi:10.5194/amt-4-1855-2011.

McCarthy, M. C., K. A. Boering, T. Rahn, J. M. Eiler, A. L. Rice, S. C. Tyler, S. Schauffler, E. Atlas, and D. G. Johnson (2004), The hydrogen isotopic composition of water vapor entering the stratosphere inferred from high-precision measurements of δD-CH_4 and δD-H_2, *J. Geophys. Res.*, *109*, D07304, doi:10.1029/2003JD004003.

Mote, P. W., K. H. Rosenlof, J. R. Holton, R. S. Harwood, and J. W. Waters (1996), An atmospheric tape recorder: The imprint of tropical tropopause temperatures on stratospheric water vapor, *J. Geophys. Res.*, *101*, 3989–4006, doi:10.1029/95JD03422.

Moyer, E. J., F. W. Irion, Y. L. Yung, and M. R. Gunson (1996), ATMOS stratospheric deuterated water and implications for troposphere-stratosphere transport, *Geophys. Res. Lett.*, *23*(17), 2385–2388, doi:10.1029/96GL01489.

Nassar, R., P. F. Bernath, C. D. Boone, A. Gettelman, S. D. Mcleod, and C. P. Rinsland (2007), Variability in HDO/H_2O abundance ratios in the tropical tropopause layer, *J. Geophys. Res.*, *112*, D21305, doi:10.1029/2007JD008417.

Notholt, J., et al. (2010), Trend in ice moistening the stratosphere—Constraints from isotope data of water and methane, *Atmos. Chem. Phys.*, *10*, 201–207, doi:10.5194/acp-10-201-2010.

Park, M., W. J. Randel, A. Gettelman, S. Massie, and J. Jiang (2007), Transport above the Asian summer monsoon anticyclone inferred from Aura MLS tracers, *J. Geophys. Res.*, *112*, D16309, doi:10.1029/2006JD008294.

Payne, V. H., D. Noone, A. Dudhia, C. Piccolo, and R. G. Grainger (2007), Global satellite measurements of HDO and implications for understanding the transport of water vapour into the stratosphere, *Q. J. R. Meteorol. Soc.*, *133*(627), 1459–1471, doi:10.1002/qj.127.

Ploeger, F., P. Konopka, G. Günther, J.-U. Grooß, and R. Müller (2010), Impact of the vertical velocity scheme on modeling transport in the tropical tropopause layer, *J. Geophys. Res.*, *115*, D03301, doi:10.1029/2009JD012023.

Randel, W. J., F. Wu, A. Gettelman, J. M. Russell III, J. M. Zawodny, and S. J. Oltmans (2001), Seasonal variation of water vapor in the lower stratosphere observed in Halogen Occultation Experiment data, *J. Geophys. Res.*, *106*, 14,313–14,325, doi:10.1029/2001JD900048.

Randel, W. J., M. Park, L. Emmons, D. Kinnison, P. Bernath, K. Walker, C. Boone, and H. Pumphrey (2010), Asian monsoon transport of pollution to the stratosphere, *Science*, *328*, 611–613, doi:10.1126/science.1182274.

Read, W. G., et al. (2008), The roles of convection, extratropical mixing, and in-situ freeze-drying in the tropical tropopause layer, *Atmos. Chem. Phys.*, *8*, 6051–6067, doi:10.5194/acp-8-6051-2008.

Remsberg, E. E., P. P. Bhatt, and J. M. Russell III (1996), Estimates of the water vapor budget of the stratosphere from UARS HALOE data, *J. Geophys. Res.*, *101*, 6749–6766, doi:10.1029/95JD03858.

Sayres, D. S., L. Pfister, T. F. Hanisco, E. J. Moyer, J. B. Smith, J. M. St. Clair, A. S. O'Brien, M. F. Witinski, M. Legg, and J. G. Anderson (2010), The influence of convection on the water isotopic composition of the tropical tropopause layer and tropical stratosphere, *J. Geophys. Res.*, *115*, D00J20, doi:10.1029/2009JD013100.

Schmidt, G. A., G. Hoffmann, D. T. Shindell, and Y. Hu (2005), Modeling atmospheric stable water isotopes and the potential for constraining cloud processes and stratosphere-troposphere water exchange, *J. Geophys. Res.*, *110*, D21314, doi:10.1029/2005JD005790.

Steinwagner, J. S., et al. (2007), HDO measurements with MIPAS, *Atmos. Chem. Phys.*, *7*, 2601–2615, doi:10.5194/acp-7-2601-2007.

Steinwagner, J. S., et al. (2010), Tropical dehydration processes constrained by the seasonality of stratospheric deuterated water, *Nat. Geosci.*, *3*(4), 262–266, doi:10.1038/ngeo822.

Stephens, G. L., et al. (2008), CloudSat mission: Performance and early science after the first year of operation, *J. Geophys. Res.*, *113*, D00A18, doi:10.1029/2008JD009982.

Urban, J., et al. (2007), Global observations of middle atmosphere water vapour by the Odin satellite: An overview, *Planet. Space Sci.*, *55*, 1093–1102, doi:10.1016/j.pss.2006.11.021.

Vömel, H., S. J. Oltmans, D. J. Hofmann, T. Deshler, and J. M. Rosen (1995), The evolution of the dehydration in the Antarctic stratospheric vortex, *J. Geophys. Res.*, *100*, 13,919–13,926, doi:10.1029/95JD01000.

Wang, P. K. (2003), Moisture plumes above thunderstorm anvils and their contributions to cross tropopause transport of water vapor in midlatitudes, *J. Geophys. Res.*, *108*(D6), 4194, doi:10.1029/2002JD002581.

Waugh, D. W., and T. M. Hall (2002), Age of stratospheric air: Theory, observations and models, *Rev. Geophys.*, *40*(4), 1010, doi:10.1029/2000RG000101.

Winker, D. M., W. H. Hunt, and M. J. McGill (2007), Initial performance assessment of CALIOP, *Geophys. Res. Lett.*, *34*, L19803, doi:10.1029/2007GL030135.

Wright, J. S., R. Fu, S. Fueglistaler, Y. S. Liu, and Y. Zhang (2011), The influence of summertime convection over Southeast Asia on water vapor in the tropical stratosphere, *J. Geophys. Res.*, *116*, D12302, doi:10.1029/2010JD015416.

Wrotny, J. E., G. E. Nedoluha, C. Boone, G. P. Stiller, and J. P. McCormack (2010), Total hydrogen budget of the equatorial upper stratosphere, *J. Geophys. Res.*, *115*, D04302, doi:10.1029/2009JD012135.

Yang, Q., Q. Fu, J. Austin, A. Gettelman, F. Li, and H. Vömel (2008), Observationally derived and general circulation model simulated tropical stratospheric upward mass fluxes, *J. Geophys. Res.*, *113*, D00B07, doi:10.1029/2008JD009945.

Zahn, A., P. Franz, C. Bechtel, J.-U. Grooß, and T. Röckmann (2006), Modelling the budget of middle atmospheric water vapour isotopes, *Atmos. Chem. Phys.*, *6*, 2073–2090, doi:10.5194/acp-6-2073-2006.

Zhang, C. (1993), On the annual cycle in highest clouds in the tropics, *J. Clim.*, *6*, 1987–1990, doi:10.1175/1520-0442(1993)006<1987:OTACIH>2.0.CO;2.

P. Bernath, Department of Chemistry and Biochemistry, Old Dominion University, Norfolk, VA 23529, USA.

C. Boone, Department of Chemistry, University of Waterloo, 200 University Ave. West, Waterloo, ON N2L 3G1, Canada.

E. Jensen, NASA Ames Research Center, MS 245-4, Moffett Field, CA 94035, USA.

E. Moyer, Department of the Geophysical Sciences, University of Chicago, Chicago, IL 60637, USA.

M. Park and W. J. Randel, National Center for Atmospheric Research, P.O. Box 3000, Boulder, CO 80307, USA. (randel@ucar.edu)

K. Walker, Department of Physics, University of Toronto, 60 St. George St., Toronto, ON M5S 1A7, Canada.